JOURNAL OF SPACECRAFT AND ROCKETS
Vol. 40, No. 5, September–October 2003
This paper reprinted from AIAA Paper 84-0223, Jan. 1984

DIRECT SIMULATION OF TRANSITIONAL FLOW FOR HYPERSONIC REENTRY CONDITIONS

James N. Moss*
NASA Langley Research Center
Hampton, Virginia 23665

Graeme A. Bird†
University of Sydney
New South Wales, Australia

Abstract

This paper presents results of flowfield calculations for typical hypersonic reentry conditions encountered by the nose region of the Space Shuttle Orbiter. Most of the transitional flow regime is covered by the altitude range of 150 to 92 km. Calculations were made with the Direct Simulation Monte Carlo (DSMC) method that accounts for translational, rotational, vibrational, and chemical nonequilibrium effects. Comparison of the DSMC heating results with both Shuttle flight data and continuum predictions showed good agreement at the lowest altitude considered. However, as the altitude increased, the continuum predictions, which did not include slip effects, departed rapidly from the DSMC results by overpredicting both heating and drag. The results demonstrate the effects of rarefaction on the shock and the shock layer, along with the extent of the slip and temperature jump at the surface. Also, the sensitivity of the flow structure to the gas-surface interaction model, thermal accommodation, and surface catalysis are studied.

Nomenclature

A_b	base area
C_D	drag coefficient, $2F_x/\rho_\infty U_\infty^2 A_b$
C_f	friction coefficient, $2\tau/\rho_\infty U_\infty^2$
C_H	heat-transfer coefficient, $2q/\rho_\infty U_\infty^3$
C_i	mass fraction of species i, ρ_i/ρ
$\tilde{C}_O$	mass fraction of element oxygen
d	nominal molecular diameter
F	force
Kn	Knudsen number, λ/ℓ
K_r^2	Cheng's parameter, $p_\infty R_N/\mu_\infty u_\infty C^* \equiv \sqrt{\pi} R_N/2S_\infty \lambda_\infty C^*$
ℓ	characteristic dimension
M	molecular weight of mixture
R_N	nose radius
R	universal gas constant, R = 8.3143 J/mol K
Re_∞	Reynolds number, $\rho_\infty U_\infty R_N/\mu_\infty$
S_∞	speed ratio, $U_\infty\sqrt{M/2R\bar{T}_\infty}$
T	thermodynamic temperature
T_{ov}	overall kinetic temperature
T*	$(T_{O,\infty} + T_W)/2$
u	velocity component tangent to body surface
U_∞	freestream velocity
X_i	mole fraction of species i
x	coordinate measured along the body centerline
x/L	nondimensionalized Space Shuttle orbital axial length
η	coordinate normal to body surface
θ	hyperboloid asymptotic half angle
λ_∞	freestream mean-free path
λ_1	mean-free path adjacent to body surface
μ	viscosity
μ*	viscosity evaluated at T*
ρ	density
σ	total collision cross section
τ	shear stress

Subscripts

i	ith species
w	wall values
∞	freestream values
σ	total values

*This work was performed under the NASA Langley Floyd L. Thompson Fellowship at The University of Sydney for 1982-83.
**Research Leader, Aerothermodynamics Branch, Space Systems Division, Member AIAA.
†Professor, Dept. of Aeronautical Engineering, The University of Sydney, Sydney, Australia, AF AIAA.

Abbreviations

DSMC direct simulation Monte Carlo

OTV orbital transfer vehicles

STS-2 space transportation system, shuttle flight number two

VSL viscous shock layer

Introduction

Currently there is a renewed interest in the aerothermodynamics of external flows about vehicles at very high altitudes. Two factors contributing to the enhanced interest are the development of the U.S. space transportation system (the Space Shuttle), and the studies underway to identify ways of enhancing the capability of the space transportation system by developing orbital transfer vehicles (OTV's) that utilize aeroassist technology[1] to achieve a specified low Earth orbit after returning from a high Earth orbit. The Space Shuttle Orbiter is now making routine flights and provides a means of conducting experiments and of making measurements throughout the flow spectrum--encompassing free-molecule through continuum flow regimes. For the aeroassisted portion of an OTV mission, the vehicle will be at very high altitudes[2-3] ($\geq$ 75 km) while traveling at speeds of about 10 to 7.5 km/s. Consequently, a portion of the atmospheric encounter of an OTV will occur in the transitional flow regime; the extent of the transitional flow encounter will depend on the aerodynamic characteristics of the vehicle. Hence, knowledge of the drag and heating experienced during the atmospheric encounter is critical in assessing the aerodynamic performance and thermal protection requirements for such a vehicle. In the transitional flow regime, both the drag and heating are very sensitive to the degree of rarefaction.

The transition flow regime, bounded by continuum and free-molecule flow, has always posed difficulties for designers who generally resort to empirical correlations based on sparse experimental data. Ground-based experimental data are not available for transitional flow conditions for atmospheric encounters at speeds of 7.5 km/s or greater. Under these conditions the speed ratio is of the order of 20, the surface temperature is of the order of 0.01 of the total temperature, and for altitudes greater than 100 km a significant amount of atomic oxygen exists in the freestream. Therefore, it is most desirable to have a computational method which can provide data for comparison with the measurements from the Shuttle.

Computationally there appears to be no alternative to the particle approach when the Knudsen number is of order unity and higher.[4] The only closed equation that is then applicable is the Boltzmann equation. Solutions of the Boltzmann equation are readily obtained in the free-molecule limit as the Knudsen number tends to infinity, but very serious analytical difficulties are encountered at Knudsen numbers characteristic of transitional flow. As a consequence of the need for an alternative approach, Monte Carlo procedures (any method that employs random numbers) have been developed. Of the various techniques for the Monte Carlo simulation of gas flows, the Direct Simulation Monte Carlo (DSMC) method is the one that is most readily applied to complex problems.[5] The DSMC method has been developed by Bird[6-7] over the past twenty years, where the applications of the method have advanced from idealized or generally artificial test cases to problems of specific engineering situations.[5,8-9]

The application of Monte Carlo simulation methods has been aimed primarily at the transition regime which is characterized by Knudsen numbers that are above the upper limit for the validity of the Navier-Stokes equations, but below the level at which the flow falls into the collisionless flow or free-molecule regime[4] (see Fig. 1). The current paper focuses on the transitional regime with special emphasis on obtaining solutions at or near conditions for which continuum solutions remain valid. The freestream conditions are those representative of the reentry conditions experienced by the Space Shuttle Orbiter during reentry and encompass an altitude range of 150 to 92 km. Comparisons of the DSMC predictions are made with Shuttle flight data for heat-transfer rates. Furthermore, comparisons with continuum predictions[10] are made for the lower altitude conditions for heat transfer, drag, and flowfield structure. Also, the impact of variations in surface catalytic activity and surface thermal accommodation on heating is demonstrated. The calculations were performed with sufficient resolution to isolate the extent of the temperature jump and velocity slip at the surface. The results represent the first transitional flow predictions for Earth reentry in which nonequilibrium effects due to translation, rotation, vibration, and chemistry are modeled in the simulation. Finally, the current study has direct implications for the studies that are being conducted to define the technology requirements for aeroassisted orbital transfer vehicles.

Analysis

The Direct Simulation Monte Carlo Method

Any method that employs random numbers may be described as a "Monte Carlo method," and there are a number of methods for which the terms "Monte Carlo" and "simulation" may be attached. In Ref. 4 Bird categorizes the various Monte Carlo simulation methods into four basic groups and outlines the features of each group.

In the DSMC method, the intermolecular collisions are dealt with on a probabilistic rather than a deterministic basis. The time parameter in the simulation may be identified with physical time in the real flow, and all calculations are unsteady. When the boundary conditions are such that the flow is steady, then the solution is the asymptotic limit of the unsteady flow. The computation is always started from an initial state that permits an exact specification such as a vacuum or uniform equilibrium flow. Consequently, the method does not require an initial approximation to the flowfield

and does not involve any iterative procedures. A computational cell network is required only in physical space rather than phase space. Furthermore, advantage may be taken of flow symmetries to reduce the dimensions of the cell network and the number of position coordinates that need be stored for each molecule, but the collisions are always treated as three-dimensional phenomena. The boundary conditions are specified in terms of the behavior of the individual molecules rather than the distribution function. All procedures may be specified in such a manner that the computational time is directly proportional to the number of simulated molecules.

References 4 and 6 review the effects of molecular complexity on the results from previous simulations in which the molecular models for monatomic gases range from the hard sphere to those including long-range attractive forces. The effects appear to be fully explained through the variation of collision cross-section with relative speed or temperature. Variations in angular scattering law do not appear to have a significant influence on any flow for which comparative data is available. Consequently, the "variable hard sphere" (VHS) model (Ref. 6) is now recommended for the simulation of monatomic gases in an engineering context. Basically, the VHS model incorporates the essential features of the more complex models while retaining the computational simplicity of the hard sphere model. The VHS model has a well defined diameter and follows the classical hard sphere scattering law, but the diameter is an inverse power law function of the relative collision energy between the colliding molecules, i.e.

$$\sigma \equiv \pi d^2 \propto (1/2\ M_r\ C_r^2)^{-\omega} \qquad (1)$$

where M_r is the reduced mass and C_r is the collision relative speed. The power law, ω, is directly related to the temperature exponent of the coefficient of viscosity (see Ref. 6).

For diatomic and polyatomic gases, the establishment of adequate models has proved to be difficult, and the difficulties associated with the physical models have led to the development of phenomenological models of which the Larsen-Borgnakke[11] model is recommended for engineering studies. The model satisfies the principle of detailed balance for translational velocities so that, when equilibrium is achieved, the translational distribution conforms to the Maxwellian, and the translational and internal temperatures are equal. An outline of the Larsen-Borgnakke phenomenological model in a form that is compatible with a gas mixture of VHS molecules is given in Ref. 6.

The classical collision theory for chemical reaction rates is essentially a phenomenological approach based on steric factors or reactive cross sections and can be readily incorporated into direct-simulation methods. The expressions for the steric factors are developed in Ref. 7 for hard spheres and inverse power law models while the results for VHS models are given in Ref. 6.

The VHS model along with the compatible Larsen-Borgnakke model and reactive cross sections are the molecular models used in the present Monte Carlo simulations.

Viscous-Shock-Layer Method

The continuum results presented for comparison purposes were obtained by solving the steady viscous-shock-layer (VSL) equations where most of the results have been reported in Ref. 10. The VSL method solves a set of equations that is uniformly valid throughout the shock layer. The VSL equations are obtained from the steady-state, Navier-Stokes equations by keeping terms up to second order in the inverse square root of a Reynolds number, i.e.

$$\varepsilon = \sqrt{\mu_{ref}/\rho_\infty U_\infty R_N} \qquad (2)$$

where μ_{ref} is the reference viscosity evaluated at a reference temperature ($T_{ref} = U_\infty^2/Cp_\infty$ where Cp_∞ is the freestream specific heat). Consequently, one set of equations is solved for both the inviscid and viscous regions (see Ref. 10 for the governing equations). The equations are solved as described by Davis[12] as an initial-value, boundary-value problem using an implicit, finite-difference, numerical procedure. Global iteration is used to relax an initial thin-shock-layer approximation and other approximations concerning the initial shock shape.

Relevant to the present study is the results of Ref. 13 where perfect gas VSL and Navier-Stokes solutions were compared for blunt body hypersonic flow with appropriate slip and jump boundary conditions. The comparison showed that the VSL method is sufficiently accurate for freestream Reynolds numbers of the order of a thousand. However, substantial difference in drag and heating (both quantities low in comparison with the Navier-Stokes results at 15 and 25 percent, respectively) occur in the stagnation region for Reynolds numbers of the order of a hundred.

Conditions for Calculations

The freestream conditions and vehicle parameters are representative of the Shuttle orbiter nose during reentry. They are summarized in Table 1. Unless stated otherwise, all results presented are for a noncatalytic wall.

Recent continuum calculations have been performed for the second shuttle flight (STS-2), and the results of these calculations have been compared with flight measurements of the heat-transfer rates along the windward centerline of the shuttle. The results reported by Shinn[10] for an altitude range of 92 to 48 km showed that the nonequilibrium viscous-shock-layer (VSL) predictions gave generally good agreement with the flight results. The results of those calculations showed that the nonequilibrium chemistry had a very pronounced effect on the predicted heating for a significant portion of the heat pulse, particularly the higher altitude portion of the heat pulse.

In order to make meaningful comparisons with existing continuum calculations, the present DSMC calculations use the same chemical kinetics model as Ref. 10 (the species O, O_2, N, N_2, and NO with

34 chemical reactions). However, as noted earlier, the rate constants have been converted to reaction cross-sections. Also, most calculations are for the windward centerline of the shuttle as modeled in Ref. 10. An "equivalent axisymmetric body" concept was used in that study to model the windward centerline of the Shuttle at a given angle of attack with an appropriate axisymmetric body at zero angle of attack. The axisymmetric body is a hyperboloid with nose radii, R_N, and asymptotic body half angles, θ, as given in Table 1. Some calculations were made for a three-dimensional shape for comparison with those from the computationally simpler axisymmetric model.

The freestream conditions for cases one and two correspond to STS-2 (space transportation system, second flight) while those for cases three and four are for STS-3. The trajectory parameters such as velocity and angle of attack were determined from a trajectory reconstruction process as described in Ref. 14. Freestream density and temperature were determined by a procedure[15] which combined atmospheric modeling and meteorological data taken close to the time of Shuttle flight. Since measured meteorological data were not available above 90 km, the Jacchia-Roberts model[16] was used in this region with the boundary values chosen to match the meteorological profiles below 90 km.[15] The uncertainty in freestream density above 90 km that results from this procedure is expected to increase with altitude, but its magnitude cannot be determined. The freestream conditions for cases five through eight are representative of those encountered by the Shuttle during reentry. For these cases, the freestream density, temperature, and composition is that given by Jacchia[16] for an exospheric temperature of 1200 K. Note that the composition was adjusted to that for three freestream species (O_2, N_2, and O). The freestream gas composition for cases three and four are also adjusted values from Jacchia while those for cases one and two are the same as used in Ref. 10.

The wall temperature distributions used for cases one through four correspond to values that were measured with thermocouples mounted in the Shuttle tile coating at various locations along the windward centerline. Furthermore, the flight heating rates were calculated from the thermocouple data by using a one-dimensional, transient heat-transfer analysis.[17] For cases five through eight, the wall temperature was assumed to be constant at 300 K.

Several freestream parameters that are often used to characterize a flowfield are included in Table 1 (c), and their definitions are given in the Nomenclature list.

A plane view of the computational domain is depicted in Fig. 2. This consists of one or more blocks of which only one block resides in core memory at a given time. Each block may consist of one or more arbitrary regions within which the time step and the weighting factor that relate the number of computational molecules to the number of physical molecules is a constant. The smallest unit of physical space is the cell which provides a convenient reference for the sampling of the macroscopic gas properties. The dimensions of the cells must be such that the change in flow properties across each cell is small. Time is advanced in discrete steps of magnitude such that the time step is small in comparison with the mean collision time.

Most calculations were performed using three blocks with two regions per block and 275 cells per block. The number of computational molecules per cell were always greater than six with the total number of molecules being approximately 16,000 for the three blocks. The computations were performed on a Perkin Elmer 3220 minicomputer with one megabyte of core memory. Using three computational blocks, no more than sixty percent of the core memory of the machine was utilized while performing the calculations. The computer run times ranged from 50 to 250 hours, depending on the freestream density.

Results and Discussion

While the results cover most of the transitional flow regime, special attention has been paid the 92.35 km case. This is because it overlaps with the apparent range of validity of the VSL continuum calculations.

Early in the study, attempts were made to isolate the sensitivity of the calculated surface heating rates to various parameters for an altitude of 92.35 km. Among those parameters considered were the effect of changing the gas phase reaction rate constants (increasing the pre-exponential constant by a factor of two relative to the nominal data set), varying the body length to investigate possible there were any "end of body" effects, checking for possible three-dimensional effects by using an elliptic paraboloid at angle of attack which gives a much better representation of the Shuttle surface curvature in the transverse plane, varying the wall temperature with respect to the measured Shuttle values, varying the computational cell dimension in the direction normal to the body surface, and changing the molecular constants that describe the collision cross section of the gas species. Of these parametric variations, only the last two significantly influenced the heat transfer at the surface.

When the molecular constants [collision cross section at a reference temperature and the exponential term in Eq. (1)] were adjusted to produce a larger collision cross section, the surface heating decreased. Future studies will be made where the molecular constants for the chemical species will be further adjusted such that the transport properties of the individual species are more closely modeled. Such a fine tuning of the molecular constants was not done in the present study, but such a process could produce changes in predicted heating of the order of 10 percent with respect to the results presented herein.

As the cell dimension normal to the surface is reduced from that of a coarse grid to one that resolves the macroscopic gradients, the predicted heating decreases because the particles (atoms and molecules) are able to adjust to local conditions rather than arriving at the surface

from larger distances and higher energies than is appropriate.

For the 92.35 km case, numerous calculations were made using different computational cell sizes. The results showed that the surface pressure was relatively insensitive while the heating and skin friction was sensitive to the cell dimension normal to the surface. The final normal cell distribution used in this study was such that approximately five computational cells were within a mean-free path of the surface, and for cells removed from the surface the thickness was less than a local mean-free path.

To achieve the aforementioned normal cell resolution, the computational requirements for case one was quite long, so a much shorter calculation was performed for this case where fifty cells were used normal to the body and a much shorter body simulated such that only six cells in the direction along the body was used. Only one block with six regions was used for these computations, and the results compared favorably (Fig. 3) with the STS-2 heating results and the VSL prediction. (The drag results for case 1 as included in Table 1 is that obtained with a coarser grid and with the computational domain as previously described for the nominal configuration.) By varying the length of the computational cells in the direction tangent to the body, (changing the length by a factor of two) little effect on predicted heating is evident (Fig. 3).

As for the structure of the flowfield, Fig. 4 presents information along the stagnation streamline for the 92 km case. The DSMC results show that, although the shock thickness is of the same order as the shock layer, the maximum temperatures for the VSL and DSMC solutions differ by only about 6 percent. [Note that two different temperatures are being compared in Fig. 4 (a). For the VSL calculations, local thermodynamic equilibrium is assumed, and therefore, only one temperature describes the translational and internal energy states. This is not necessarily the case for the DSMC calculation where thermodynamic nonequilibrium effects are modeled. The temperature shown for the DSMC solution is an overall kinetic temperature, T_{ov}, defined as the weighted mean of the translational and internal temperature (See Ref. 7).] The overall temperature begins to rise appreciably at a distance of about 0.4 meters from the body while the VSL calculation, using a discontinuous shock, has a total shock layer thickness of 0.1 meters. When the individual temperature components are examined for the DSMC solution [Fig. 4 (b)], the rotational and vibrational temperatures are seen to lag far behind the translational temperatures. The difference between the translational and internal temperature modes increases with altitude since the collision rate decreases. In the region adjacent to the surface, the slope of the temperature profile resulting from the two computational methods [Fig. 4 (c)] are slightly different, and the temperature jump predicted is 350 K.

The density rise will always lag the temperature rise as evidenced by the results in Figs. 4 (a) and 4 (d). In fact, if one assumes that the center of the shock for the DSMC calculation is at the location where the density equals the mean of the freestream and post shock continuum values, then the continuum and DSMC shock locations are in good agreement.

The chemical composition profiles along the stagnation streamline resulting from the DSMC and VSL solutions are presented in Figs. 4 (e) and 4 (d) for O_2 and N_2, and N, respectively. The profile resulting from the two solutions has the same general shape; however, the DSMC results show a significant influence of the thick shock wave on the chemical composition within the shock layer. A significant number of chemical reactions occur in the shock wave, producing atomic mass fraction in excess of twenty percent at the shock location as given by the continuum solution. By including shock slip boundary conditions in the VSL solution, the chemical composition profile would compare more favorably with the DSMC results within the shock layer as is demonstrated by the recent study of Shinn.[18]

The effect of increasing the altitude is to create a more rarefied situation in which the shock layer and shock wave merge [Figs. 5 (a) and 5 (b)]. As the altitude increases, the extent of the flowfield disturbance continues to increase as evidenced by the results shown in Fig. 5 (c). Shown are the stagnation locations for the maximum value of overall temperature and the location where the density is six times the freestream density (perfect gas condition) as a function of freestream density. Since the collision rate is proportional to the square of the density, the rate of chemical reactions decreases with increasing altitude and the present calculations show little chemical activity occuring above 105 km.

Effect of Rarefaction on Surface Quantities

Quantities of particular interest in the transitional flow regime are the heating and drag experienced by a vehicle. Figures 6 (a) and 6 (b) present the stagnation-point heating results expressed in terms of the heat-transfer coefficient as a function of the freestream Knudsen number and Cheng's rarefaction parameter, respectively. The predicted results show the qualitative behavior expected in that the heat-transfer coefficient increases rapidly with increasing rarefaction and approaches a value of one as the free molecule limit is approached. Also shown in Fig. 6 is a comparison of the DSMC results with those obtained with a VSL method. The VSL results presented are for altitudes of 78.9, 85.7, 92.4, and 99.5 km. The comparison shows that the VSL results, without slip and jump boundary conditions, begin to depart rapidly from the DSMC results for λ_∞/R_N of about 0.03 or K_r^2 of about 7. Both the DSMC and VSL methods are in good agreement with the flight measured results at 92.35 km.

Comparisons such as presented in Fig. 6 provide information on where a continuum method such as the VSL method fails to provide correct surface quantities. The effect of including slip and jump boundary conditions in the VSL analysis is discussed in a concurrent study by Shinn.[18]

The comparison of the drag prediction (Fig. 7) shows trends similar to those discussed for the heat-transfer comparisons. As was the case for the heat-transfer coefficient, the drag coefficient experiences a significant increase in value with increasing rarefaction. The change in drag is due primarily to the increase in skin friction rather than a change in pressure coefficient. The extent of the change in skin friction distribution with increasing altitude is presented in Fig. 8 (a). The corresponding heat-transfer distributions are given in Fig. 8 (b).

As the density of a flow is reduced from that of continuum conditions, the conditions of temperature continuity adjacent to the surface and zero surface velocity are no longer satisfied. This occurs because the state of the molecules adjacent to the surface is affected not only by the surface but also by the flow conditions at a distance of the order of a mean-free path from the surface. Consequently, as the flow becomes more rarefied, the spatial region that influences the state of the gas adjacent to the surface increases and gives rise to significant velocity slip and temperature jump effects. In figures 9 and 10, the calculated temperature jump and velocity slip are presented as a function of Knudsen number. Figure 9 presents the stagnation temperature jump expressed as a fraction of the specified wall temperature, and the values range from 0.33 to 4.64 for the Knudsen number range considered. The velocity slip shown in Fig. 10 is for an axial location of 1.5 m, and the values when expressed as a fraction of the freestream velocity range from about 0.010 to 0.028.

Comparison with Flight Data

The DSMC heating results show good agreement with the corresponding flight results for the 92.35 km case. However, as the altitude is increased, the agreement between calculated and flight-deduced heating rates becomes progressively worse. Figure 11 shows a comparison of these results between 92 and 110 km--that is, the early portion of the orbiter heating pulse. The heat-transfer rates are presented as a function of altitude in Fig. 11 (a) while the same results when expressed in terms of heat-transfer coefficient and freestream Knudsen number are shown in Fig. 11 (b). These results are for x/L location of 0.025 where the value of x is the distance measured from the nose of the orbiter and L is the distance from the orbiter nose to the hinge line (L = 32.9 m). The orbiter x/L location of 0.025 corresponds to the hyperboloid x location of approximately 0.2 m.

When both the flight and calculated heating values are expressed in terms of the heat-transfer coefficient and compared in terms of the freestream Knudsen number, the differences become very apparent as shown in Fig. 11 (b). The flight heat-transfer coefficient values increase with increasing Knudsen number up to an altitude of 105 km and then remain constant at a value of 0.22 rather than having an increasing trend with increasing Knudsen number as does the DSMC results. The trend of the measured C_H values is in conflict with the free molecule limit with complete accommodation as well as with the DSMC results.

The reason for the flight C_H trend with increasing Knudsen number is not presently known. However, two areas of concern are obvious; one being the accuracy of the flight heating values at low heating conditions [Fig. 11 (a)], and the second is that some event may occur in flight that has not been included in the Monte Carlo simulation. The accuracy of the flight heating data is not addressed in the present study as they have been discussed previously.[17] Therefore, if it is assumed that the thermocouple measurements and the heating rates deduced from those measurements are reasonably accurate, then the question arises of the cause of the apparent low heating values for Knudsen numbers of the order of 0.1 and greater. Two events that would produce lower heating values are mass addition to the flowfield and the lack of full thermal accommodation. If there is any outgassing as the orbiter encounters the onset of the heating pulse, then this would reduce the heating. (It should be noted that a fuel dump occurs prior to entry where the fuel for the reaction control surfaces in the nose region is ejected forward of the orbiter.) The effect of mass addition was not considered in the present calculations; however, the effect of the surface reflection model was examined.

Effect of Surface Reflection Model

For case 4, an altitude of 110 km, a calculation was made assuming that half of the particles that interact with the surface do so in a diffuse manner with full thermal accommodation and half interact in a specular manner (elastic collisions) with no thermal accommodation. The net result is a thermal accommodation of 0.5. The results of this calculation are compared with those from the diffuse calculation in Figs. 11 and 12. The stagnation-point heating is 60 percent of that for full accommodation. Similar reductions in heating are evident at other locations downstream of the stagnation point [Fig. 12 (a)]. Even with the assumption of 50 percent specular reflection, the calculated heating is high in comparison with the STS-3 flight results for x/L locations of 0.025, 0.098, and 0.140. Therefore, it is concluded that the flight heating results cannot be explained in terms of surface reflection model alone since the thermal accommodation coefficient required to achieve agreement with flight data would be much less than 0.5.

Altering the gas-surface interaction model produces a substantial change in the state of the gas adjacent to the surface. The impact on the overall temperature adjacent to the surface is to produce a temperature jump that is about 4.5 times that for the diffuse surface with full accommodation [Fig. 12 (b)]. However, the slope of the temperature profiles are very similar as is shown for the stagnation point in Fig. 12 (c).

Catalytic Wall Effect

In general, two conditions must be met before wall catalytic activity has an influence on surface heating. First, the energy of the flowfield must be such as to create dissociated flow and second, some degree of chemical nonequilibrium must persist. Such conditions exist for

much of the Shuttle entry heating pulse and will also exist for an aeroassist orbital transfer vehicle during atmospheric encounter.

In the present study, the catalytic wall effect was examined for only the 92.35 km case. The results of those calculations are shown in Fig. 13 where the stagnation-point heating is presented as a function of the surface recombination probability γ_i. In the present calculations, the recombination probability was assumed to be the same for both atomic oxygen and nitrogen even though different values could be specified for the respective species. For the noncatalytic surface, the heating is 65 percent of the fully catalytic value which indicates the advantage of having a surface that is basically noncatalytic.

Values of the recombination probability appropriate for the Shuttle tiles have been measured by Scott[19] for the atomic species oxygen and nitrogen. For the 92.35 km case where the stagnation wall temperature is 1043 K, the γ_i values using Scott's results would be 0.007 and 0.0004 for nitrogen and oxygen, respectively. Consequently, the results for the noncatalytic surface are very nearly appropriate to the Shuttle tiles.

Concluding Remarks

Results obtained with the DSMC method for the transitional flow regime encountered by the Shuttle during reentry demonstrate the practical application of the method to such problems. The solutions obtained show good agreement at the lowest altitude case (92.35 km) with both flight and VSL heating results. With increasing altitude, the agreement between flight and calculated heating becomes progressively poorer. While the calculated heat-transfer coefficient asymptotically approaches a value of 1.0 for large Knudsen number, the flight results never reach a value much greater than 0.22. If an energy accommodation coefficient less than 1.0 is assumed, the agreement is improved, but the discrepancy cannot be totally resolved with realistic values of accomodation coefficient. Significant temperature jump and velocity slip effects are present in all cases. Chemical reactions within the flowfield are evident up to an altitude of about 105 km, whereas at higher altitudes the gas composition is basically that of the freestream. Thermodynamic nonequilibrium effects are evident for all conditions considered, extending all the way to the surface at the higher altitudes. The results for heating and drag suggest that continuum calculations must be modified to account for slip and temperature jump effects at freestream Knudsen numbers of approximately 0.03.

Future studies should focus on the sensitivity of heating, drag, and flowfield structure to variations in molecular constants. Also, it would be of interest to extend the present calculations to lower altitudes for comparison with the results from continuum calculations. The molecular constants in the DSMC method should be further refined so that the two numerical methods use as near as possible the same transport properties.

References

[1] Walberg, D. G., "Aeroassisted Orbit Transfer - Window Opens on Missions," Astronautics and Aeronautics, November 1983, pp. 36-43.

[2] Shinn, J. L., and Jones, J. J., "Chemical Nonequilibrium Effects on Flowfields for Aeroassist Orbital Transfer Vehicles" AIAA Paper 83-0214, January 1983.

[3] Howe, J. T., "Introductory Aerothermodynamics of Advanced Space Transportation Systems," AIAA Paper 83-0406, January 1983.

[4] Bird, G. A., "Monte Carlo Simulation of Gas Flows," Annual Reviews of Fluid Mechanics, Vol. 10, edited by M. D. Van Dyke et al., Annual Reviews Inc., Palo Alto, 1979, p. 11.

[5] Bird, G. A., "Simulation of Multi-Dimensional and Chemically Reacting Flows," Rarefied Gas Dynamics, Vol. 1, CEA, Paris, 1979.

[6] Bird, G. A., "Monte-Carlo Simulation in an Engineering Context," AIAA Progress in Astronautics and Aeronautics: Rarefied Gas Dynamics, Vol. 74, Part 1, edited by Sam S. Fisher, 1981, pp. 239-255.

[7] Bird, G. A., Molecular Gas Dynamics, Clarendon Press, Oxford, 1976.

[8] Hueser, J. E. and Brock, F. J., "Shuttle Flow Field Analysis using the Direct Simulation Monte Carlo Technique," paper presented at the USAF/NASA International Spacecraft Contamination Conference, USAF Academy, Colorado, March 1978.

[9] Chrusciel, G. T. and Pool, L A., "Knudsen Layer Characteristics for a Highly Cooled Blunt Body in Hypersonic Rarefied Flow," AIAA Paper 83-1424, June 1983.

[10] Shinn, J. L., Moss, J. N., and Simmonds, A. L., "Viscous-Shock-Layer Heating Analysis for the Shuttle Windward Plane with Surface Finite Catalytic Recombination Rates," AIAA Paper 84-0842, June 1982.

[11] Borgnakke, Claus and Larsen, Paul S., "Statistical Collision Model for Monte Carlo Simulation of Polyatomic Gas Mixtures," Journal of Computational Physics, Vol. 18, 1975, pp. 405-420.

[12] Davis, R. T., "Numerical Solution of the Hypersonic Viscous Shock-Layer Equations," AIAA Journal, Vol. 8, No. 5, May 1970, pp. 843-351.

[13] Anderson, E. C. and Moss, James N., "Numerical Solution of the Steady-State Navier-Stokes Equations for Hypersonic Flow About Blunt Axisymmetric Bodies," NASA TM X-71977, June 1974.

[14] Compton, H. R., Findlay, J. T., Kelly, G. M., and Heck, M. L., "Shuttle (STS-1) Entry Trajectory Reconstruction," AIAA Paper 81-2459, November 1981.

[15]Price, J. M. and Blanchard, R. C., "Determination of Atmospheric Properties for STS-1 Aerothermodynamic Investigations," AIAA Paper 81-2430, November 1981.

[16]Jacchia, L. G., "Thermospheric Temperature, Density, and Composition: New Models," Research in Space Science, SAO Special Report No. 375, March 1977.

[17]Throckmorton, D. A., "Benchmark Aeroheating Data From the First Flights of the Space Shuttle Orbiter," AIAA Paper 82-0003, January 1982.

[18]Shinn, J. L. and Simmonds, A. L., "Comparison of Viscous-Shock-Layer Heating Analysis with Shuttle Flight Data in Slip Flow Regime," AIAA Paper 84-0226, January 1984.

[19]Scott, C. D., "Catalytic Recombination of Oxygen and Nitrogen in High Temperature Reusable Surface Insulation," Progress in Astronautics and Aeronautics: Aerothermodynamics and Planetary Entry, edited by A. L. Crosbie, Vol. 77 of 1981, pp. 192-212.

Table 1. Conditions and Results

(a) Freestream Conditions

Case	Altitude, km	Density, kg/m^3	U_∞, km/s	T_∞, K	Mole Fractions X_{O_2}	X_{N_2}	X_O	$\bar{M}$, g/mol	λ_∞, m
1	92.35	2.184×10^{-6}	7.50	180	.217	.783	0	28.96	.036
2	99.49	5.906×10^{-7}	7.50	190	.217	.783	0	28.96	.134
3	104.93	2.457×10^{-7}	7.47	223	.153	.782	.065	27.85	.309
4	109.75	1.146×10^{-7}	7.47	249	.123	.771	.106	27.23	.649
5	115.00	4.380×10^{-8}	7.50	304	.098	.754	.148	26.63	1.659
6	122.50	1.790×10^{-8}	7.50	401	.080	.723	.197	25.98	3.961
7	130.00	8.230×10^{-9}	7.50	500	.071	.691	.238	25.44	8.438
8	150.00	2.140×10^{-9}	7.50	733	.055	.615	.330	24.27	30.964

Table 1. Continued

(b) Body* Parameters and Wall Temperature

Case	R_N, m	θ, deg	Wall Temperature Range, k From	To
1	1.296	41.15	1043	800
2	1.362	42.50	800	610
3	1.362	42.50	560	453
4	1.362	42.50	420	374
5	1.362	42.50	300	300
6	1.362	42.50	300	300
7	1.362	42.50	300	300
8	1.362	42.50	300	300

*Hyperboloid with asymptotic half angle θ and nose radius R_N.

Table 1. Concluded

(c) Various Parameters and Results

Case	Re_∞	Kn_∞	K_r^2	S_∞	q, kW/m^2	C_H	C_D
1	1751.	.028	7.667	23.3	81.3	.176	1.24
2	475.	.098	2.210	22.7	49.9	.405	1.27
3	172.	.227	1.739	20.5	30.5	.595	1.36
4	73.	.476	.508	19.2	16.6	.687	1.52
5	24.	1.219	.213	17.2	7.7	.838	1.69
6	8.	2.909	.097	14.8	3.3	.874	1.82
7	3.1	6.196	.048	13.1	1.6	.927	1.89
8	0.6	22.734	.014	10.6	0.4	.964	1.94

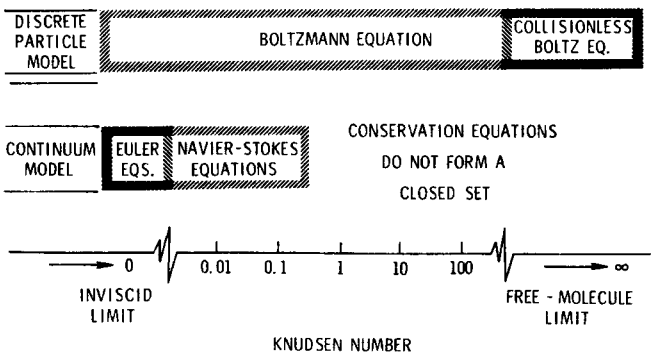

Fig. 1 The Knudsen-number limits on the conventional mathematical models of neutral gas flows.

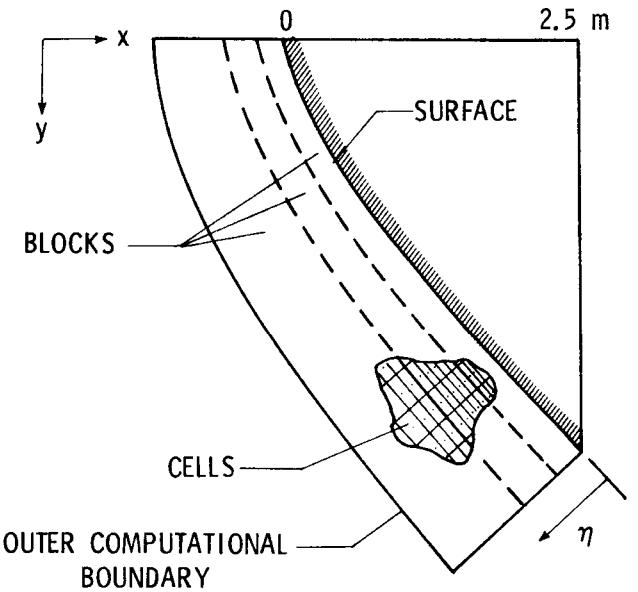

Fig. 2 Computational domain.

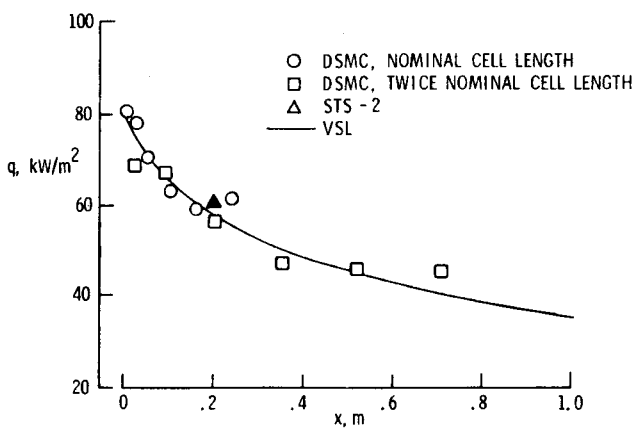

Fig. 3 Comparison of predicted and measured heating (Alt = 92.35 km).

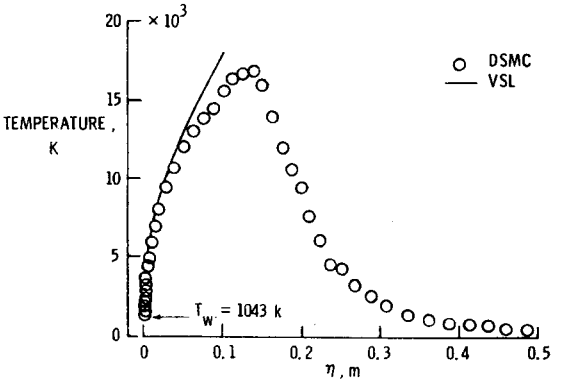

(a) Comparison of temperature.

Fig. 4 Flowfield structure along stagnation streamline (Alt = 92.35 km).

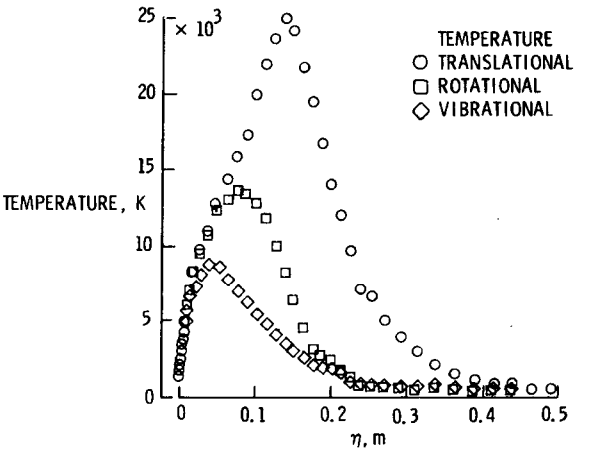

(b) Extent of thermodynamic nonequilibrium.

Fig. 4 Continued.

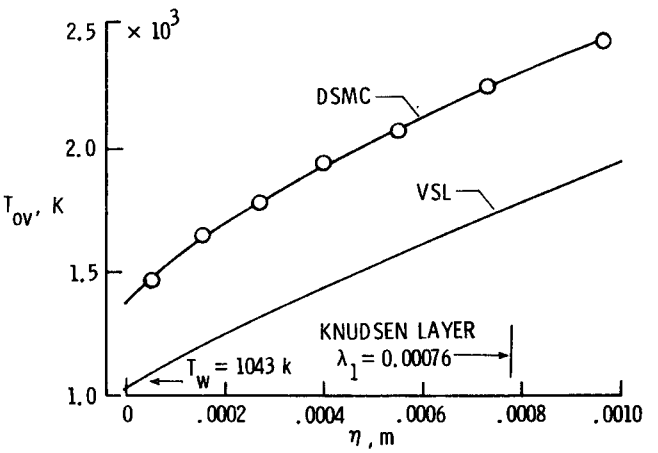

(c) Comparison of temperature profiles adjacent to surface.

Fig. 4 Continued.

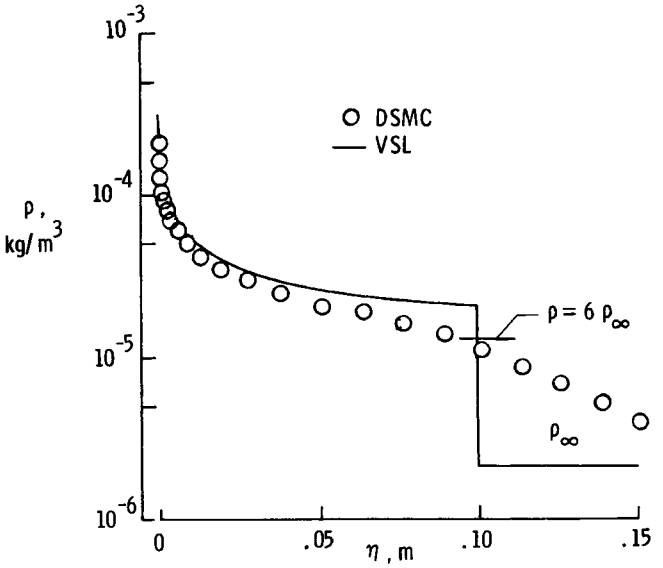

(d) Comparison of density profiles.

Fig. 4 Continued.

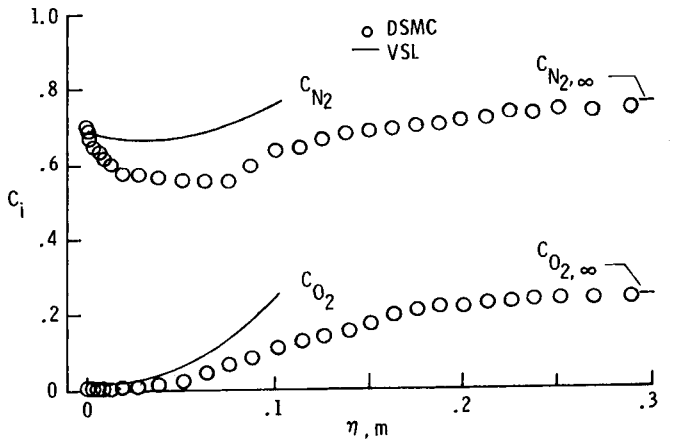

(e) Comparison of species mass fraction profiles for N_2 and O_2.

Fig. 4 Continued.

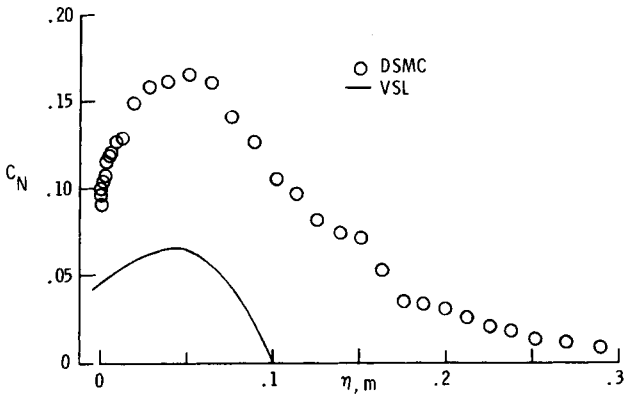

(f) Comparison of species mass fraction profiles for atomic nitrogen.

Fig. 4 Concluded.

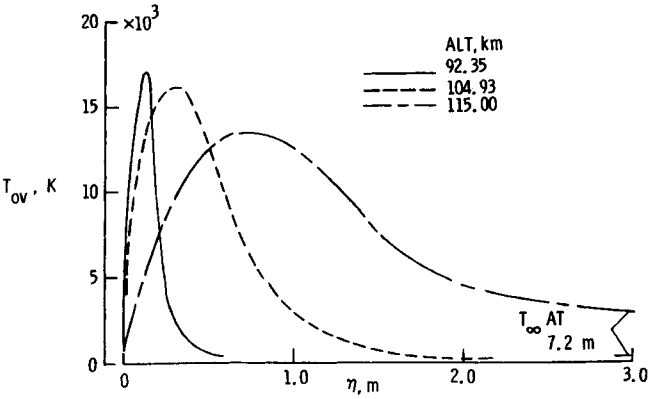

(a) Overall kinetic temperature profiles.

Fig. 5 Effect of rarefaction on flowfield structure (stagnation streamline).

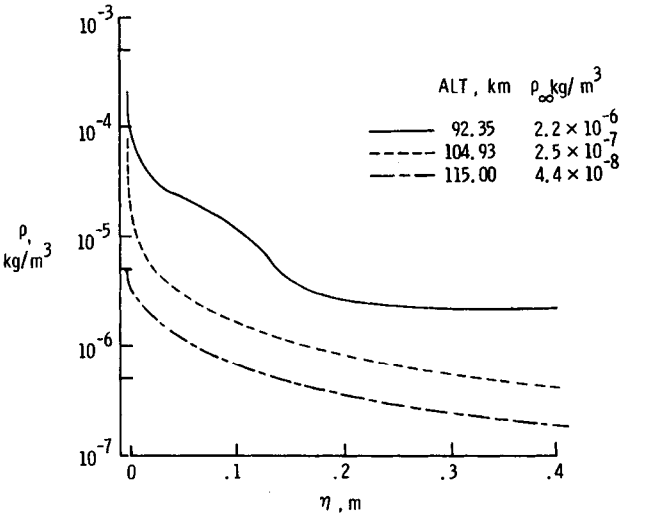

(b) Density profiles.

Fig. 5 Continued.

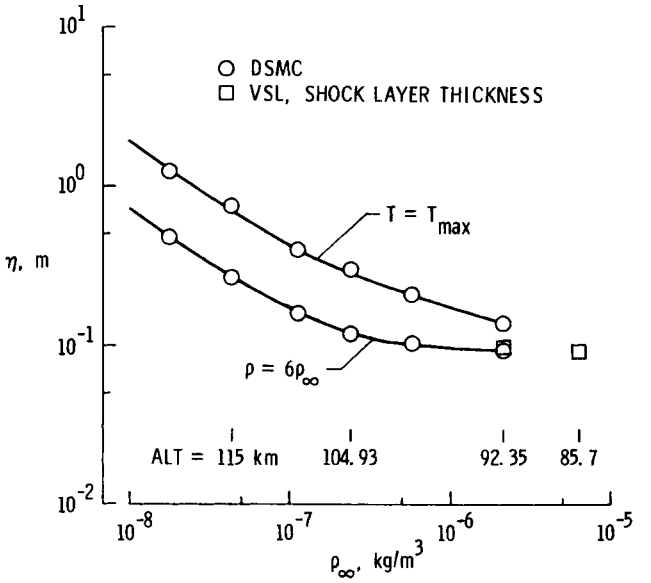

(c) Location of stagnation-point quantities.

Fig. 5 Concluded.

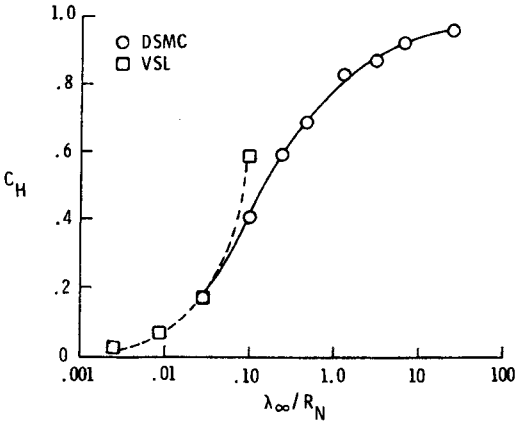

(a) Heat-transfer coefficient versus Knudsen number.

Fig. 6 Comparison of predicted stagnation-point heating.

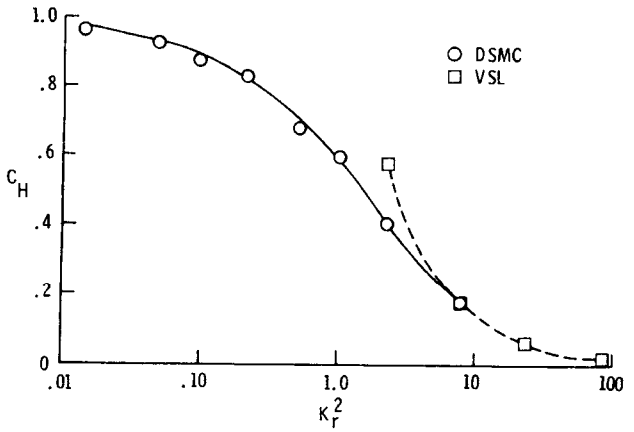

(b) Heat-transfer coefficient versus Cheng's rarefaction parameter.

Fig. 6 Concluded.

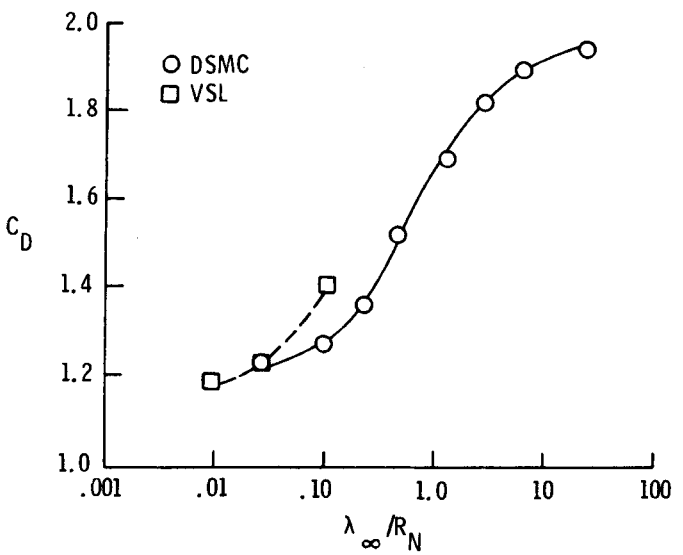

Fig. 7 Effect of rarefaction on predicted drag.

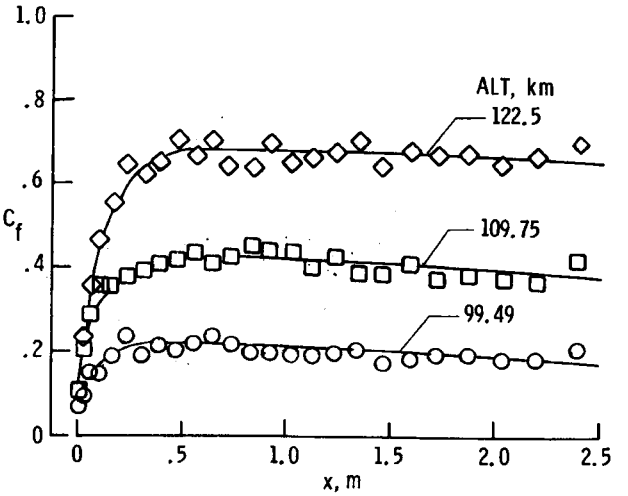

(a) Skin friction coefficient.

Fig. 8 Effect of rarefaction on surface distributions.

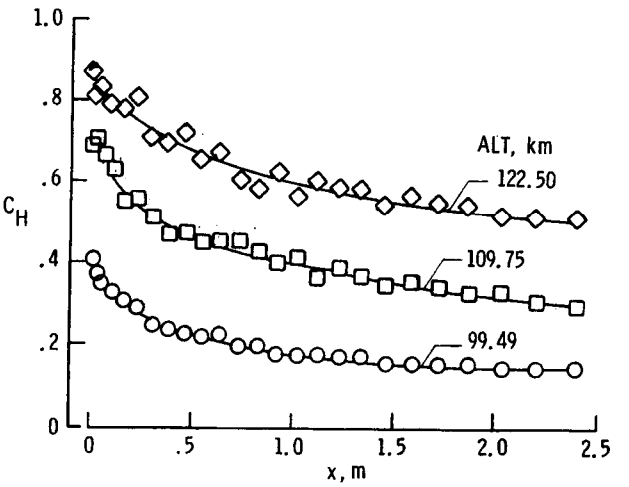

(b) Heat-transfer coefficient.

Fig. 8 Concluded.

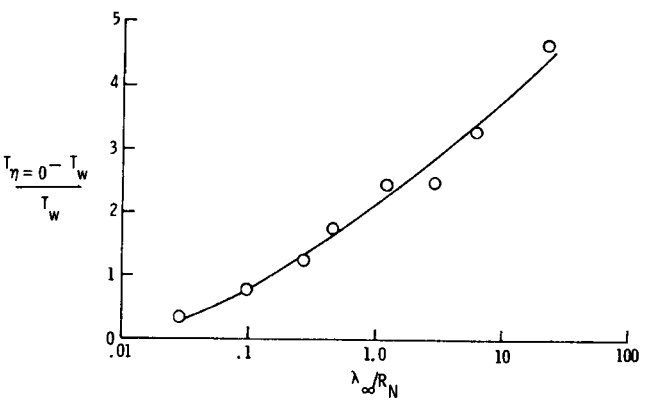

Fig. 9 Effect of rarefaction on stagnation-point temperature jump.

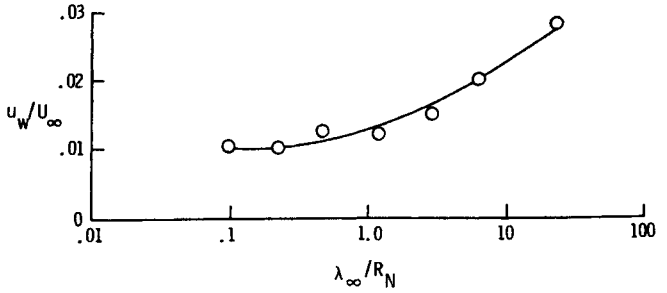

Fig. 10 Effect of rarefaction on velocity slip (X = 1.5 m and $U_\infty \simeq 7.5$ km/s).

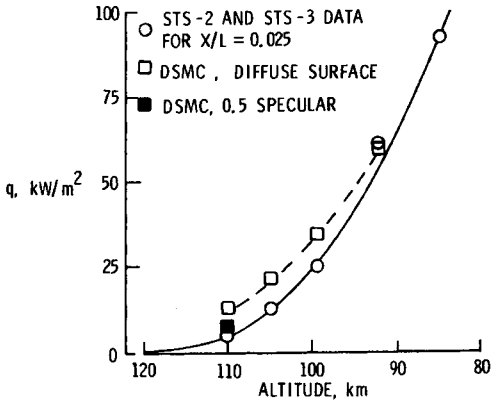

(a) Heating rate versus altitude.

Fig. 11 Comparison of flight data with DSMC predictions.

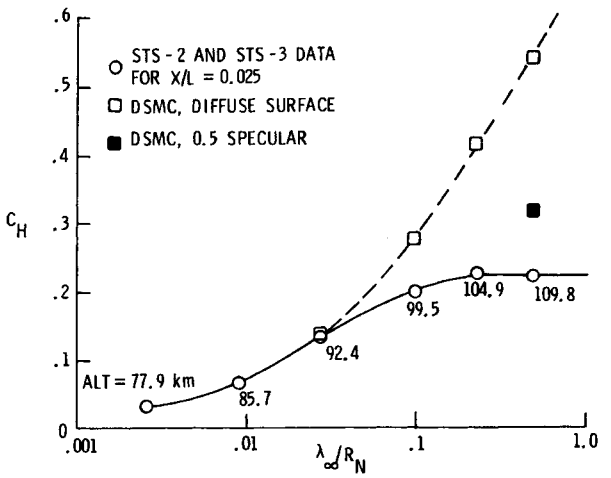

(b) Heat-transfer coefficient versus Knudsen number.

Fig. 11 Concluded.

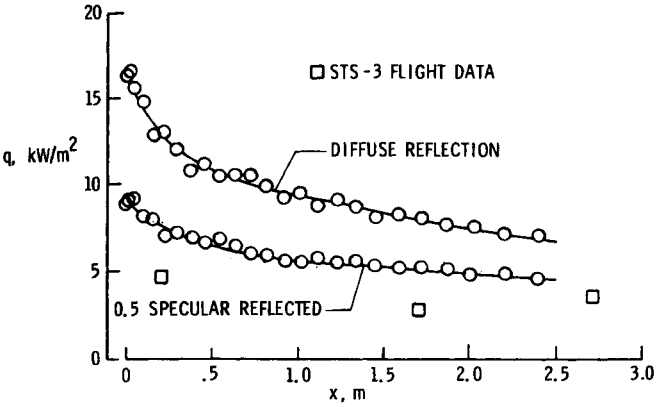

(a) Heat-transfer distribution.

Fig. 12 Effect of surface reflection model (Alt = 109.95 km).

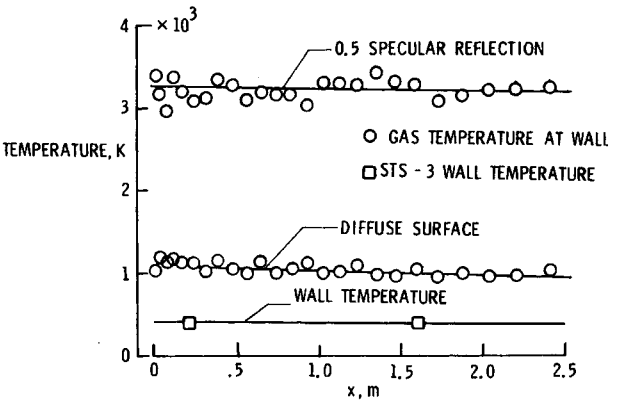

(b) Temperature jump.

Fig. 12 Continued.

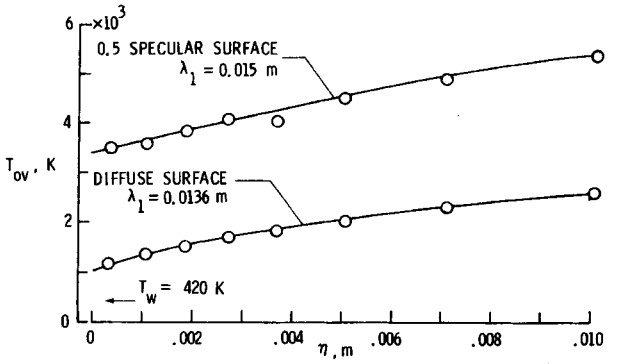

(c) Temperature profile (stagnation point).

Fig. 12 Concluded.

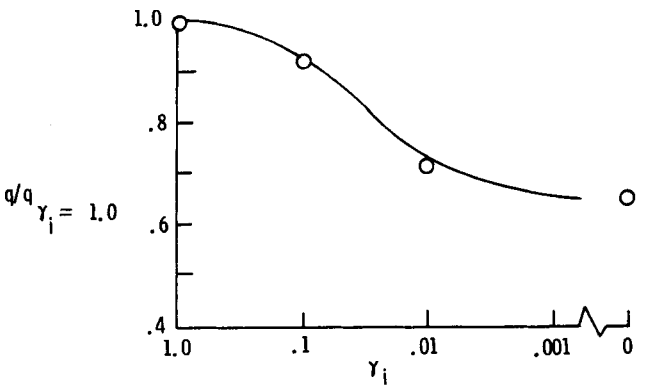

Fig. 13 Effect of surface catalysis on heating (Alt = 92.35 km, stagnation point).